# How to predict the location of the defect levels induced by 3d transition metal ions at octahedral sites of aluminate phosphors

Qu, Bingyan; Zhou, Rulong; Wang, Lei; Dorenbos, Pieter

**DOI**
10.1039/C8TC05401K

**Publication date**
2019

**Document Version**
Accepted author manuscript

**Published in**
Journal of Materials Chemistry C

Journal of
Materials Chemistry C

Accepted Manuscript

This article can be cited before page numbers have been issued, to do this please use: B. Qu, R. Zhou, L. Wang and P. Dorenbos, *J. Mater. Chem. C*, 2018, DOI: 10.1039/C8TC05401K.




ROYAL SOCIETY OF CHEMISTRY

rsc.li/materials-c

View Article Online
DOI: 10.1039/C8TC05401K

# How to predict the location of the defect levels induced by 3d transition metal ions in octahedral sites of aluminate phosphors

Bingyan Qu[a], Rulong Zhou[a], Lei Wang*[a, b] and Pieter Dorenbos*[b]

a School of Materials Science and Engineering, Hefei University of Technology, Hefei, Anhui 230009, P. R. China

b Faculty of Applied Sciences, Delft University of Technology, Mekelweg 15, 2629 JB Delft, The Netherlands

*Corresponding author: Lei Wang leiwang@hfut.edu.cn and Pieter Dorenbos p.dorenbos@tudelft.nl.



## Abstract

How the 3d transition metal (TM) ions induce defect levels in wide band gap compounds and how these defect levels evolve from compound to compound is very important in understanding and predicting the luminescent properties of TM activated phosphors. This issue is discussed by studying the ground state $3d^n$ level locations of the TM impurity ions (Sc-Zn) incorporated in octahedral sites of many oxides. These ground states $3d^n$ level locations are obtained by collecting the CT bands from literature in the past 50 years and also by the First-principle calculations. By taking the vacuum level as reference, we scale all the location of TM ion in 3+ and 2+ states and constructed a zig-zag-curve scheme in α-$Al_2O_3$ through connecting the $3d^n$ ground state energies for Sc to Zn. The scheme can be extended to other aluminates easily and so offers a first estimate on where TM level are located in compounds without complicated theoretical calculations. The estimate can be improved to a higher accuracy if the position of the valence band is known. Our work provides new insight for understanding the luminescent behavior of 3d-TM doped phosphors and may aid in developing 3d ions doped functional materials further.

View Article Online
DOI: 10.1039/C8TC05401K





## Introduction

In the past decades, phosphors have been intensively investigated because of their applications in laser materials[1], displays[2], light emitting diodes (LED) [3-5], persistent luminescent materials[6-9] etc. In these phosphors, the lanthanide (Ln) ions and 3d transition metal (3d-TM) ions are the most common luminescent centers. The locations of the electronic levels of these ions with respect to the host bands, e.g. conduction band (CB) and valence band (VB), are imperative for understanding the optical properties of phosphors and their relevant performance. For example, significant quenching would happen for d orbitals if the excitation states locate in the CB[10], or the ground states in the VB[5]. In the persistent luminescent process, if the ground states are just above the VB, the corresponding ions could act as hole trapping centers[11], and if the ground states are close to the CB, the corresponding ions may serve as electron trapping centers[9]. The energy transfer might happen if the defect levels of different ions are matched, typically $Mn^{4+}$ and $Fe^{3+}$[5]. But how to determine or predict these level locations in compounds has always remained difficult.

The location of a lanthanide ion electronic ground state $4f^n$ level in different compounds with respect to the VB may vary strongly. However, if the vacuum level is taken as the reference energy, these level locations show small and predictable variation with type of compound. The above finding is a result of the chemical shift model developed in 2012 by Dorenbos[12]. The level location with respect to the vacuum level is defined as the vacuum referred binding energy (VRBE). The double zigzag like shape of the VRBE curve that connect the $4f^n$ ground state energies for La to Lu appears remarkably invariant with type of compound. This is very useful in predicting lanthanide impurity level locations in a given compound[13]. Whether the $3d^n$-TMs follow a similar invariant and therewith predictive curve is still an open question. Once the systematics is known it will aid in understanding and developing new 3d-TM doped

View Article Online
DOI: 10.1039/C8TC05401K

phosphors further[14-16].

The 3d orbital electrons are more sensitive to the crystal field than the 4f orbital electrons, because 3d orbitals extend to the outside of the ion while the 4f orbitals are screened by outer shell 5s and 5p orbitals. Both the strength (depending on the type of the anion and bond lengths between the TM ion and the anion) and type (depending on anion coordination configuration) of the crystal field in the phosphors have large influence on the defect level energies. So, to obtain a universal rule of the VRBE of 3d-TM ions is expected to be a more difficult task than for the lanthanides. Luckily, in most of the 3d-TM doped phosphors, the crystal field experienced by the 3d-TM ions can be mainly classified into an octahedral, or tetrahedral crystal field. So, if we limit our consideration to one type of crystal field and to one type of anion, a common systematics of the VRBEs may be revealed.

In this work, we focus our attention on the VRBEs of the 3d-TM ions doped in the aluminates with octahedral crystal field. The compounds selected are $\alpha$-$Al_2O_3$ and $Y_3Al_5O_{12}$ (YAG), since experimental data of 3d-TM ions in these compounds are relatively abundant. Both the experimental data collection from literature and first-principle calculations are carried out. The results show that a common systematics of the VRBEs in the $3d^n$ ground state of 3d-TM in the octahedral crystal field of those aluminates indeed exists. Finally, we attempt to extend these two curves to other aluminates with octahedral crystal field. The obtained zigzag like curve scheme provides us a tool to predict 3d-TM level locations in compounds and so offers a guideline value for understanding and developing new phosphors with target properties.

## Method

Experimentally, we do not have tools to determine the VRBE of an electron in an impurity level routinely. We do have tools to determine energies with respect to the host bands. The energy of charge (electron) transfer (CT) between TMs and host bands can be probed by optical spectroscopy, and thermoluminescence may provide the depth

of an electron or hole trapped in a TM[17]. The CT band energy $E^{CT}(M,n)$ of $M^{n+}$ (M represents one of the 3d-TM ions) in oxides is the energy needed for an electron to optically transfer from $O^{2-}$ to $M^{n+}$, reducing $M^{n+}$ into $M^{(n-1)+}$. Our calculated electronic structures of $Al_2O_3$ and YAG show that the VB are dominated by the $O^{2-}$ 2p orbitals (see Fig. S1 in Electronic Supporting Information, ESI). $E^{CT}(M,n)$ describes the energy difference between the acceptor level of $M^{n+}$ (denoted as $M^{n+/(n-1)+}$) and the valence band maximum (VBM)[17]. Thus, the VRBE E(M,n-1) of an electron when in the acceptor level of $M^{n+/(n-1)+}$ and $E^{CT}(M,n)$ satisfies the following formula:

$$E(M,n-1) = E_V + E^{CT}(M,n) \qquad (1)$$

where $E_V$ is the energy of the VBM (the vacuum level is taken as the reference). Note, that here we use a notation that is equivalent as what is often used for the lanthanides.

Theoretically, we calculate the total energies and electronic structures of M doped α-$Al_2O_3$ and YAG by using the VASP 5.3 code[18, 19], where the projector augment wave (PAW) [20] pseudopotentials are adopted to describe the interactions of atoms. The generalized gradient approximation (GGA)[18] with exchange-correlation functional following the approach of Perdew-Burke-Ernzerhof (PBE)[20] is selected. In order to describe the valence electrons of Ti, V, Cr, Mn and Fe more accurately, the semi core p states are treated as valence. For Sc, both the semi core s and p states are treated as valence. A set of plane wave functions with the energy cutoff of 400 eV is used to describe the electronic wave functions.

The Al ions in α-$Al_2O_3$ are coordinated by six O ions, while in YAG both six- and four-coordinated Al sites are present. In our calculation, a supercell containing 2×2×2 unit cells of α-$Al_2O_3$ with the stoichiometry of $Al_{32}O_{48}$ and a primitive unit cell ($Y_{12}Al_{20}O_{48}$) of YAG is adopted. A Γ-centered 4×4×4 k-mesh is selected for k-point sampling. The defective structural models of α-$Al_2O_3$ and YAG are constructed by substituting one of the six-coordinated Al ions by an M ion. This M ion should be in 3+ state in the neutral structural models. To obtain the M ion in 4+ or 2+ state, an additional electron is taken from or added to the defective structural models. The formation energy

View Article Online
DOI: 10.1039/C8TC05401K

$E_F$ of M ion in these charge states are obtained, based on the following formula[21]:

$$E_F(M^{n+}) = E^{n-3}(M) - E(undoped) + \mu_{Al} + \mu_M + (n-3)\,\varepsilon_f, \quad (2)$$

where $E(undoped)$ represents the total energy of the undoped compound and $E^{(n-3)}(M)$ stands for the energy of the $M^{n+}$-doped compound. n-3 is the net charge of the defective structural model. For the case of $Mn^{4+}$-doped α-$Al_2O_3$, the net charge of the system n-3 is 1+ and the charge state of Mn ion is 4+. $\mu_M$ and $\mu_{Al}$ are the chemical potentials of bulk M and Al, respectively. $\varepsilon_f$ is the chemical potential of the electron and here equal to the Fermi level. The optical transition level energy (OTL) from $M^{n+}$ (denoted as initial state) to $M^{(n-1)+}$ (denoted as final state) is defined as[21]:

$$\varepsilon_f(M^{n+/(n-1)+}) = [E^{n-4}(M) - E^{n-3}(M)] - E_{VBM}. \quad (3)$$

$E_{VBM}$ is the energy at the VBM as is offered by VASP, where the vacuum level is not the reference energy. This OTL energy describes the energy needed for an electron to transfer from the VBM to $M^{n+}$, resulting into the M ion in (n-1)+ state. So, the process underlying OTL $\varepsilon_f(M^{n+/(n-1)+})$ from first principle calculation should be physically the same to that of $E^{CT}(M,n)$ from optical spectroscopy. In the calculations of OTL $\varepsilon_f(M^{n+/(n-1)+})$, the structure of the initial state $M^{n+}$-doped compound is fully relaxed, and the final state $M^{(n-1)+}$-doped compound is calculated with the same structure to that of $M^{n+}$-doped compound[21].

## Results and discussions

Table 1 lists the experimental data relevant to the CT bands of M ions with both trivalent and tetravalent charge state in α-$Al_2O_3$. These data are collected from the relevant literature of the past 50 years. Table 1 shows that for an M ion usually more than one value is listed. The overlap between CT band with inter-configurational transitions observed in absorption/excitation spectra, often complicates proper assignment. Such experimental limitations results in different reported values with large uncertainty. We list most of those experimental data for reference. For $Mn^{3+}$, the

experiment provides the onset or threshold of the CT band (4.15 eV) [22], while values for other TM refer to the energy at the peak of the CT bands. Considering that the widths of the CT bands are typically 1 eV, the CT peak energy of $Mn^{3+}$ is estimated to be about 4.65 eV. We adopt the symbol * to distinguish such estimated value. Ref. [23] described two different CT data for $Co^{3+}$, one is 3.1 eV measured at 1000 K and the other one is 3.7 eV at 77 K. For $Cu^{3+}$ and $Zn^{3+}$, unfortunately, we did not found CT data. For the tetravalent ions, only the experimental CT band energies for $Ti^{4+}$, $V^{4+}$ and $Mn^{4+}$ could be found in literature.

**Table 1** The CT data of M ions incorporated in $Al_2O_3$ and YAG. All energies are in eV.

| | $Al_2O_3$ | | $Y_3Al_5O_{12}$ | |
|---|---|---|---|---|
| | 3+ | 4+ | 3+ | 4+ |
| Sc | 8.1[24] | --- | 6.67[25] | --- |
| Ti | 7.04[26], 7.67[26],7.0[22] | 4.4[27], 4.56[28], 5.4[29] | --- | 4.8±0.3[30] |
| V | 5.75[22] | 3.76[31] | --- | 3.28[31], >3.1[32] |
| Cr | 6.94[22], 6.90[33] | --- | 6.66[#16] | 2.76[34] |
| Mn | 4.65*[22] | 3.91[35] | --- | 4.20[36], 4.0[37] |
| Fe | 4.80[22, 38], 4.60[39] | --- | 4.86[40], 4.88[41] 5.04[42], 4.75[42] | --- |
| Co | 3.10[23], 3.7[23] | --- | --- | --- |
| Ni | 3.16[22], 4.13[23] | --- | 3.50 [43, 44] | --- |

*estimated from the threshold energy of CT band.

#estimated from defect levels of $Cr^{3+}$ obtained through TL measurements.

For CT data of M doped YAG, only those of Sc, Cr, Fe and Ni in the trivalent charge state and Ti, V, Cr and Mn in the tetravalent state are available (Table 1). In YAG, M ions may be at lattice sites with either octahedral or tetrahedral crystal fields. In Table 1, all the data pertain to octahedral sites except possibly for $V^{4+}$, for which the site occupied has not been specified in experiments[31,45]. The CT energy to $Sc^{3+}$ [16, 46, 47] may be underestimated, since there is considerable mixing of the 3d-orbital with the orbitals at the nearby lying YAG band edge. The CT data of $Cr^{3+}$ are not clear, and the value of

6.66 eV is indirectly estimated from thermoluminescence (TL) glow peak analysis by Ueda et al[16]. Combining the CT energies with the VRBE at the VBM of $Al_2O_3$ (-9.6 eV) and YAG (-9.38 eV[48]), the VRBE in the ground state of the $M^{(n-1)+}$ ions in $Al_2O_3$ and YAG are obtained.

These data are not yet enough to construct the complete VRBE curve of 3d-TM electrons in octahedral crystal field in α-$Al_2O_3$. We therefore calculate the OTL of $M^{n+}$ doped α-$Al_2O_3$ using first-principle calculations. The calculated OTL together with the experimental acceptor level energies extracted from CT values are shown in Fig.1. All the calculated electronic structures of M doped α-$Al_2O_3$ can be found in part B of the ESI. The charge state of Zn will be discussed at the end of this section.

In Fig.1, the data from the OTL of $\varepsilon_f(M^{3+/2+})$ and $\varepsilon_f(M^{4+/3+})$ are represented by circle and square symbols, respectively, while the data for the experimental acceptor levels of $M^{3+}$ and $M^{4+}$ are denoted as plus (+) and cross (×) symbols. In order to compare the OTL data of $\varepsilon_f(M^{3+/2+})$ with the experimental data, the calculated results have been shifted upwards by about 0.77 eV. Although this calculation systematically underestimates experimental values, the GGA-PBE calculation can work well in predicting the trend of the CT energies of 3d-TM ions from Sc to Zn.

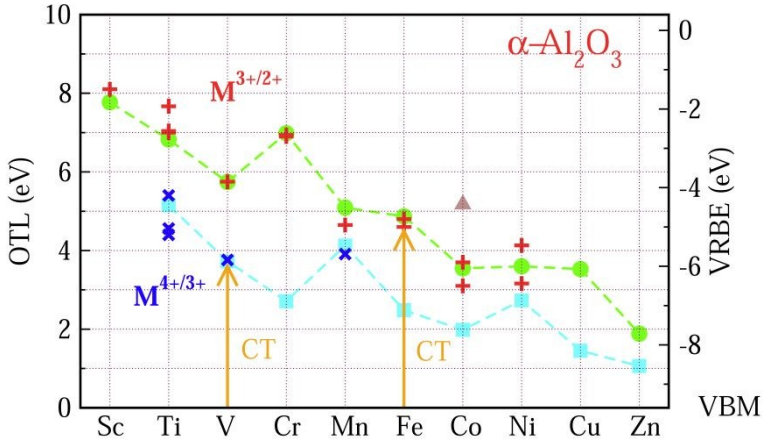


**Figure 1** (Color online) The OTL and VRBE of M ions in α-$Al_2O_3$. The circle and square symbols represent the OTL of $\varepsilon_f(M^{3+/2+})$ and $\varepsilon_f(M^{4+/3+})$, respectively. The plus and cross symbols represent experimental acceptor levels of $M^{3+}$ and $M^{4+}$ in α-$Al_2O_3$. The triangle is the OTL $\varepsilon_f(Co^{3+/2+})$ with low-spin state (see below). The arrows indicate the process of CT.

For OTL $\varepsilon_f(M^{3+/2+})$ (the upper curve in Fig.1), we find that except for Cr, the OTL decreases with the increase of the atomic number from Sc to Zn. This result is reasonable, since the OTL is related with the defect levels, which may inherit from the 3d orbitals of 3d-TM atoms. Like the 3rd ionization potentials of the free TM atoms, the binding energy of the 3d electron in 3d-TM atoms decreases with the growing number of the nuclear charge. For $Cr^{3+/2+}$, the OTL is about 1.2 eV higher than that of $V^{3+/2+}$. As shown in Fig.S4 in ESI, $V^{3+}$ has two valence electrons in the spin-up low triplet states. The OTL $\varepsilon_f(V^{3+/2+})$ describes the energy needed to transfer an electron from VBM to $V^{3+}$ ion. This electron should be accommodated in the spin-up low triplet states. However, $Cr^{3+}$ (Fig.S5) has three valence electrons that already fully occupy the spin-up low triplet states, and so the electron from the VBM has to occupy either the spin-up high doublet states or the spin-down triplet states (the OTL in these two cases are different by 0.043 eV). Obviously, this needs much more energy than in the case of $V^{3+}$. This is why $\varepsilon_f(Cr^{3+/2+})$ is about 1.2 eV larger than that of $\varepsilon_f(V^{3+/2+})$.

The good agreement of OTL $\varepsilon_f(M^{3+/2+})$ with the experimental CT band energies $E^{CT}(M,3)$ of trivalent TMs gives us confidence that also the CT band energies $E^{CT}(M,4)$ of tetravalent TM ions can be predicted by the GGA-PBE calculations. From the experimental side, we only found CT data on $Ti^{4+}$, $V^{4+}$ and $Mn^{4+}$ in $Al_2O_3$. The OTL $\varepsilon_f(M^{4+/3+})$ curve reproduces those CT data, if it is lifted by 1.566 eV. The overall trend is that the $\varepsilon_f(M^{4+/3+})$ decreases from Ti to Zn. The $\varepsilon_f(Mn^{4+/3+})$ is more than 1 eV larger than $\varepsilon_f(Cr^{4+/3+})$. $Mn^{4+}$ ion has like $Cr^{3+}$ three valence electrons, and the added electron has to occupy the higher energy doublet state. Also $\varepsilon_f(Ni^{4+/3+})$ is higher than that of its neighbors. This can also be explained from the filling of the 3d-orbitals. As shown in Fig.S9, the $Ni^{4+}$ has six valence electrons which fully occupy the low triplet states with both spin-up and spin-down. The added electron has again to occupy the higher energy doublet states.

Comparing the two OTL curves, one observes that when the lower curve is shifted leftwards by one element these two curves run nearly parallel, except for the data points of $\varepsilon_f(Ni^{4+/3+})$ and $\varepsilon_f(Co^{3+/2+})$. The reason is that similar $3d^n$ configurations are now

compared. For two M ions with the same electron configuration, the value for the lower curve is about 2.5 eV lower than that in the upper curve. This difference is a direct consequence of the higher ionic charge. Although both $Ni^{4+}$ and $Co^{3+}$ have six valence electrons, their electronic configurations are different. As shown in Fig.S8 and Fig.S9 in ESI, five valence electrons of $Co^{3+}$ occupy the spin-up states with one valence electron locating at the low spin-down triplet states, resulting in a local magnetic moment of 4 $\mu_B$ at $Co^{3+}$. This state is consistent with the experimental ground state of $t^4e^2$ [23]. We denote this state as high-spin state. For $Ni^{4+}$, six valence electrons occupy the lower triplet states with both spin orientations, and thus the local magnetic moment of $Ni^{4+}$ is 0 $\mu_B$. So this state is labeled as the low-spin state. The OTL of $Co^{3+}$ in the low-spin state has also been calculated, which is about 1.626 eV higher than that of the high-spin state as shown in Fig. 1 (the triangle).

Considering the similarity of OTL $\varepsilon_f(M^{n+/(n-1)+})$ and CT band energies $E^{CT}(M,n)$, the VRBE E(M,n-1) is also computed from the OTL $\varepsilon_f(M^{n+/(n-1)+})$. The results are shown in Fig. 1 with the right side y-axis. Through connecting these OTL or VRBE values, we obtain the zig-zag like curves of OTL (VRBE) of M ions in $\alpha$-$Al_2O_3$.

Fig. 2 shows the VRBE curves of 3d-TM ions in YAG by using the experimental data listed in Table 1 and first-principle calculations. All the electronic structures are shown in ESI. In Fig. 2, the OTL of $\varepsilon_f(M^{3+/2+})$ and $\varepsilon_f(M^{4+/3+})$ in YAG are represented by circle and square symbols, respectively, while the corresponding experimental acceptor levels are denoted as plus (+) and cross symbols (×). The VRBE is shown in Fig. 2 on the right side y-axis. The resulting $\varepsilon_f(Sc^{3+/2+})$, $\varepsilon_f(Ti^{3+/2+})$ and $\varepsilon_f(Cr^{3+/2+})$ are inaccurate and the reason is discussed in part C of ESI. In Fig.2, we adopt open symbols to distinguish $\varepsilon_f(Sc^{3+/2+})$, $\varepsilon_f(Ti^{3+/2+})$ and $\varepsilon_f(Cr^{3+/2+})$ from other OTL. For the upper curve, the energy difference between the OTL of $\varepsilon_f(Fe^{3+/2+})$ and $\varepsilon_f(Ni^{3+/2+})$ agrees well with the experiments after the calculated OTL are shifted upwards by 0.656 eV. For more evidence, we also calculate OTL of Fe ions in tetrahedral site and the difference of $\varepsilon_f(Fe^{3+/2+})$ at tetrahedral and octahedral sites is only -0.14 eV, while the CT of Fe ions in these two sites are experimentally the same[40]. For the lower curve, the calculated

View Article Online
DOI: 10.1039/C8TC05401K

results are shifted upwards by 1.357 eV.

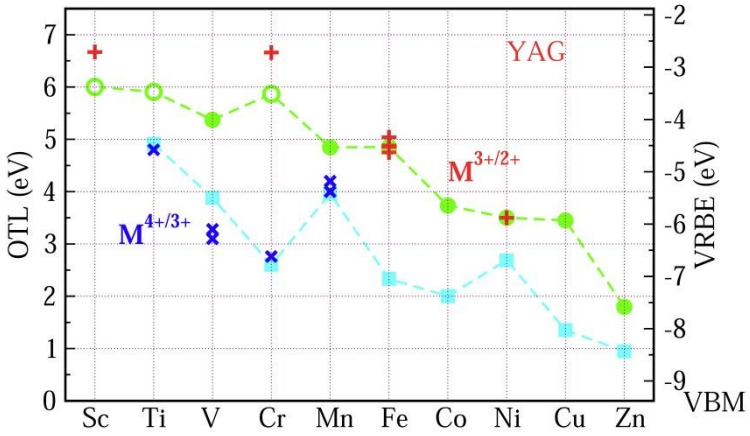


**Figure 2** (Color online) The OTL and VRBE of M ions in YAG. The circle and square symbols represent OTL of $\varepsilon_f(M^{3+/2+})$ and $\varepsilon_f(M^{4+/3+})$, respectively, where the open and full symbols denote the accurate and inaccurate results. The plus and cross symbols represent acceptor levels of 3d-TM ions with 3+ and 4+ in YAG extracted from the CT data. Note, the coordination of $V^{4+/3+}$ are not specified in literature.

Comparing Fig.2 with Fig.1, we find the VRBE curves are very similar to each other. So, we replot these VRBE curves in Fig. 3 for comparison. Here, the VRBE of $\varepsilon_f(M^{3+/2+})$ and $\varepsilon_f(M^{4+/3+})$ in α-$Al_2O_3$ are represented by the circle and square symbols, while in YAG by up and down triangles. The VRBE curves of M in both YAG and α-$Al_2O_3$ are almost parallel respectively, except the underestimated values for $Sc^{3+/2+}$, $Ti^{3+/2+}$ and $Cr^{3+/2+}$ in YAG.

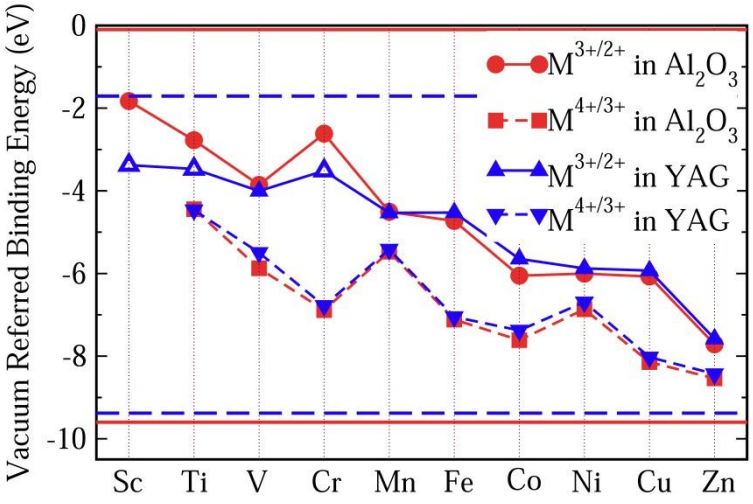


**Figure 3** (Color online) The VRBE of M ions in α-$Al_2O_3$ and YAG. The circle and square symbols

represent VRBE of $\varepsilon_f(M^{3+/2+})$ and $\varepsilon_f(M^{4+/3+})$ in α-$Al_2O_3$, while the up and down triangle represent VRBE of $\varepsilon_f(M^{3+/2+})$ and $\varepsilon_f(M^{4+/3+})$ in YAG. The horizontal lines represent experimental VBM (lower) and conduction band minimum (upper) of $Al_2O_3$ (solid line) and YAG (dash line).

The similarity of VRBE curves in α-$Al_2O_3$ and YAG can be understood from molecular orbital theory. As shown in Fig. 4, the 3d orbitals of the M ion couple with ligand bonds. The ligand bonds are fully occupied and are from the bonding orbitals of O ions and cations, such as $Al^{3+}$ in α-$Al_2O_3$ or $Y^{3+}$ and $Al^{3+}$ in YAG. The combination of the ligand bonds with $d_{x^2-y^2}$ or $d_{z^2}$ orbital forms σ bonding orbital with the lowest energy (denoted as e) and σ antibonding orbital (e*) with the highest energy. Between these orbitals are t and t*, which are π bonding and antibonding orbital originating from the coupling of $d_{xy}$, $d_{xz}$ or $d_{yz}$ with ligand bonds. The e and t orbitals are lower in energy than the ligand bonds and are fully occupied by the electrons from the ligand bonds. (Theoretically, electrons are indistinguishable, but we notionally indicate the electrons as being derived from the ligands or 3d-TM for the purpose of filling in energy-level diagram.) The t* and e* orbitals have higher energies, and appear in the band gap as defect levels. The 3d-electrons from M ion will go to fill t* and e* orbitals. So the energies of t* or e* dominate 3d-TM VRBE. As we limited M ions to octahedral site, the factors that affect VRBE are the size of $AlO_6$ and the energies of ligand bonds. The average Al-O bond length is 191.5 pm in α-$Al_2O_3$ and 192 pm for the octahedral Al site in YAG. The ligand bonds in the crystal form VB. As shown in Fig. S1 in ESI, the VB of both compounds have a width of about 7 eV with the VBM at about -9.6 eV for α-$Al_2O_3$ and -9.38 eV for YAG (here the reference energy is the vacuum level). Thus, the defect levels of M ions in these two compounds are similar to each other and then also the VRBE of 3d-TM.

View Article Online
DOI: 10.1039/C8TC05401K

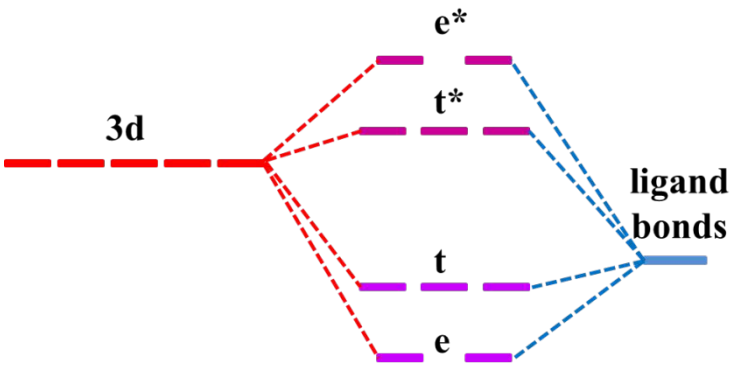


**Figure 4** (Color online) Schematic energy level diagram for transition metal in octahedral site of α-$Al_2O_3$ and YAG. Not drawn to scale.

As shown in Fig. 5(a), the Al-O bonds in α-$Al_2O_3$ are about 186 pm and 197 pm (calculated result) with O-Al-O angles of about 79.71°, 90.736°, and 101.17°, which have large deviation from the perfect Al-O octahedron. For the octahedron in YAG, the O-Al-O angles are 93.20° and 86.80° (Fig.5(b)) which is more close to perfect. However, the VRBE of 3d-TM in these two compounds are very similar. These results imply that the distortion of crystal field has little influence on VRBE.

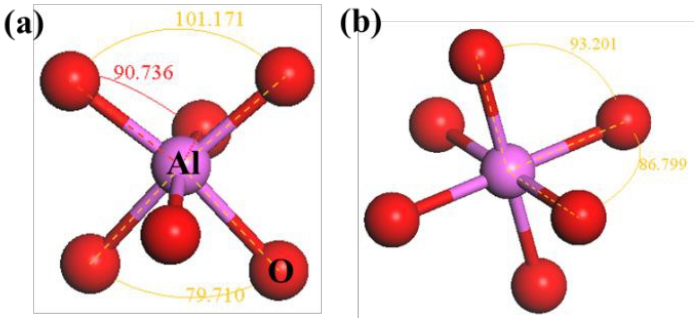


**Figure 5** (Color online) The Al-O octahedron in (a) α-$Al_2O_3$ and (b) YAG with different crystal field distortions. The data present the angle of adjacent O-Al bonding.

Although the VRBE curve of 3d-TMs in YAG is similar to that in α-$Al_2O_3$, they are not exactly the same as seen in Fig.3. The question then arises how to predict the VRBE of 3d-TMs in other aluminates with octahedral sites. Considering the relatively scarce CT data of 3d-TM in a specify aluminate, it is difficult to obtain a complete VRBE curve like α-$Al_2O_3$ and YAG. Yet, to obtain the VRBE of a given 3d-TM ion on octahedral site in different aluminates seems to be feasible. Rogers and Dorenbos have reported that the VRBEs of $Ti^{4+/3+}$ in many different oxides fall within ±1 eV from the

View Article Online
DOI: 10.1039/C8TC05401K

mean value of -3.95 eV[49]. For $Mn^{4+}$, $Fe^{3+}$ and $Cr^{3+}$ in oxides, we collected in Table 2 the CT band energies, and the corresponding VRBEs for $Mn^{4+/3+}$, $Fe^{3+/2+}$ and $Cr^{3+/2+}$ are shown in Fig. 6. For $Mn^{4+/3+}$, the compounds cover aluminates plus the zirconate $CaZrO_3$. The average acceptor VRBE value is -4.82 eV with a spread of ±0.8 eV. Since the $O^{2-}$ - $Mn^{4+}$ CT band is very broad and there is often a strong overlap between the $^4A_{2g} \rightarrow {}^4T_{1g}$ band and the CT band, it is difficult to determine the precise CT peak position.

Fig. 6(b) shows that the average VRBE of $Fe^{3+/2+}$ is -4.50 eV in aluminates with a spread ±0.4 eV. We also collected the VRBEs of $Fe^{3+/2+}$ in other oxides, like $Y_3Ga_5O_{12}$, MgO, α-$Ga_2O_3$ and the titanate $BaTiO_3$, and find that those values are quite well consistent with that average value. We take the average value (-4.58 eV) covering all the $Fe^{3+}$-doped oxides listed in Table 2 as the VRBE of $Fe^{3+/2+}$ with a spread about ±0.4 eV.

The VRBE of $Cr^{3+/2+}$ locates at about -2.45 eV with a range of ±0.3 eV, as shown in Fig. 6(c). This value does not cover β-$Ga_2O_3$ and $ZnGa_2O_4$, since the acceptor level of $Cr^{3+}$ is very close to their conduction bands. So, it is difficult to distinguish the CT bands of $Cr^{3+}$ from the host absorption. In some literature[50, 51], the host band absorptions of β-$Ga_2O_3$ and $ZnGa_2O_4$ were regarded as the CT bands as shown in Fig. 6(c). In these cases, the actual VRBE value could be largely underestimated. Similar situation may happen for $Sc^{3+}$-doped compounds[14].

View Article Online
DOI: 10.1039/C8TC05401K



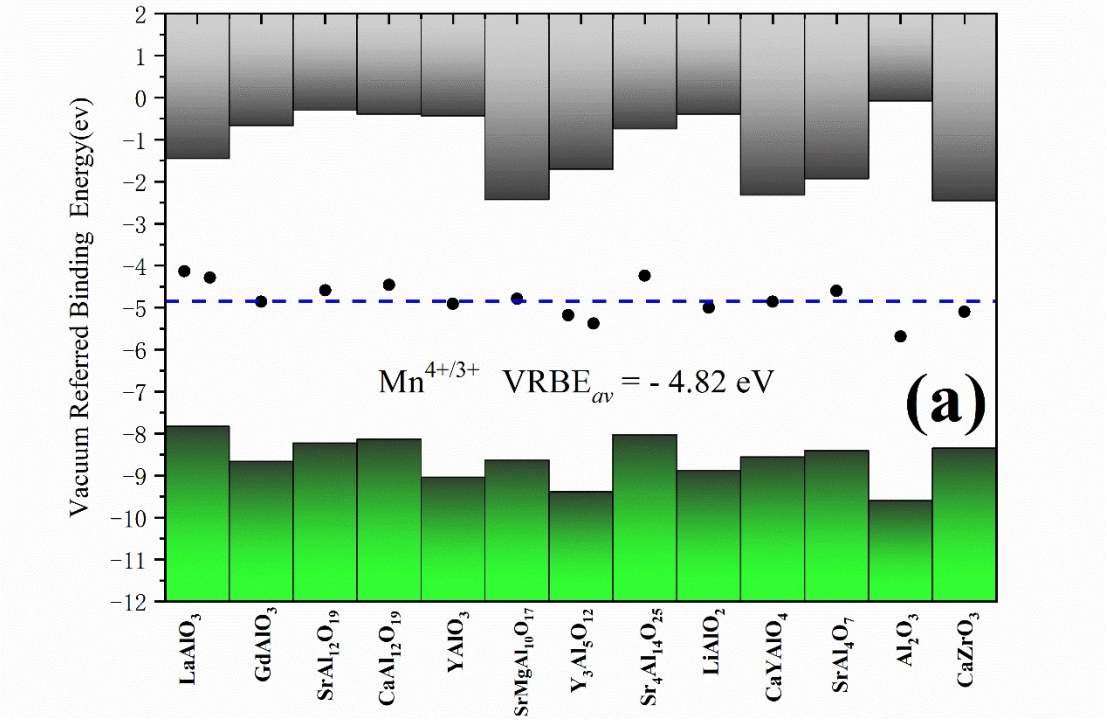


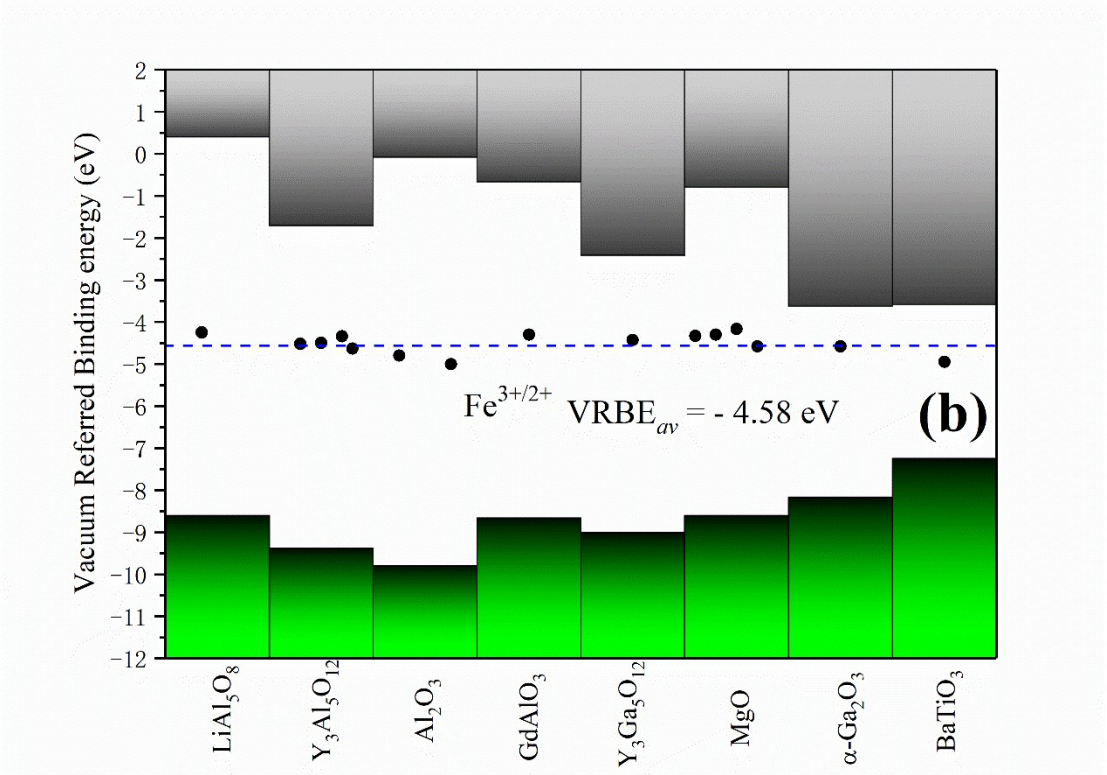

View Article Online
DOI: 10.1039/C8TC05401K

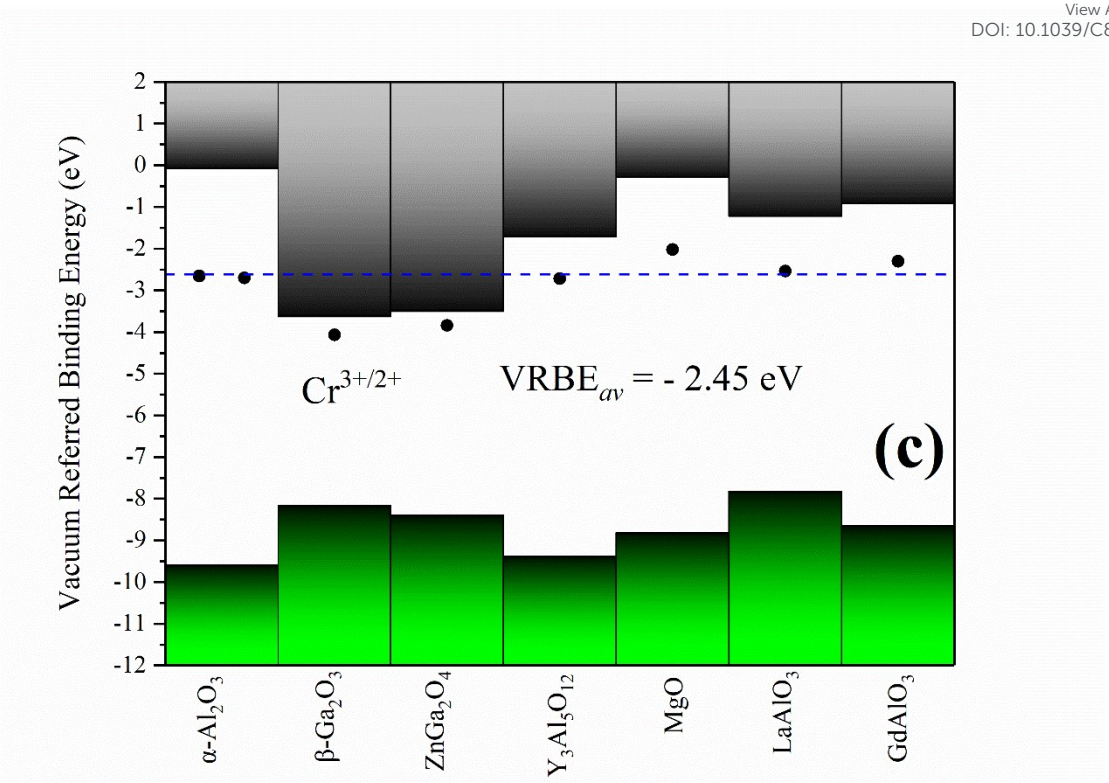


**Figure 6** Stacked VRBE schemes for acceptor levels of $Mn^{4+/3+}$, $Fe^{3+/2+}$ and $Cr^{3+/2+}$ in different phosphors. The valence and conduction bands are represented by the bottom and top bars, respectively. The solid data point is the VRBE of those acceptor levels in specific compound. The horizontal dashed line denotes the average VRBE for those acceptor levels.

**Table 2.** Experimental data on CT energies from $O^{2-}$ to $Mn^{4+}$, $Fe^{3+}$ and $Cr^{3+}$ ($E^{CT}$) in different compounds and the corresponding VRBE values. The VRBE of the conduction band minimum and valence bands maximum ($E_C$ and $E_V$), found from Rogers and Dorenbos[49, 52] or obtained from Dorenbos's Chemical Shift Model[12], are also listed. All energies are in eV.

| ions | Host | $E^{CT}$ | $E_V$ | $E_C$ | VRBE |
|---|---|---|---|---|---|
| $Mn^{4+}$ | $LaAlO_3$ | 3.69[53], 3.54[54] | -7.83 | -1.45 | -4.14,-4.29 |
| | $GdAlO_3$ | 3.80[55] | -8.66 | -0.67 | -4.86 |
| | $SrAl_{12}O_{19}$ | 3.69[56] | -8.23 | -0.30 | -4.54 |
| | $CaAl_{12}O_{19}$ | 3.67[57] | -8.13 | -0.40 | -4.46 |
| | $YAlO_3$ | 4.13[58] | -9.04 | -0.44 | -4.91 |

View Article Online
DOI: 10.1039/C8TC05401K





| | | | | | |
|---|---|---|---|---|---|
| | $SrMgAl_{10}O_{17}$ | 3.84[59] | -8.63 | -2.43 | -4.79 |
| | $Y_3Al_5O_{12}$ | 4.20[36], 4.0[37] | -9.38 | -1.71 | -5.18, -5.38 |
| | $Sr_4A1_{14}O_{25}$ | 3.79[60] | -8.03 | -0.74 | -4.24 |
| | α-$LiAlO_2$ | 3.88[61] | -8.88 | -0.4 | -5.00 |
| | $CaYAlO_4$ | 3.70[62] | -8.56 | -2.32 | -4.86 |
| | $SrAl_4O_7$ | 3.81[63] | -8.41 | -1.93 | -4.60 |
| | α-$Al_2O_3$ | 3.91[35] | -9.60 | -0.08 | -5.69 |
| | $CaZrO_3$ | 3.25[64] | -8.35 | -2.46 | -5.10 |
| $Fe^{3+}$ | $LiAl_5O_8$ | 4.35[65] | -8.6 | 0.4 | -4.25 |
| | $Y_3Al_5O_{12}$ | 4.86[40] , 4.88[41], 5.04[42], 4.75[42] | -9.38 | -1.71 | -4.52,-4.50, -4.34,-4.63 |
| | $Y_3Ga_5O_{12}$ | 4.64[66] | -9.01 | -2.42 | -4.37 |
| | α-$Al_2O_3$ | 4.80[22, 38], 4.60[39] | -9.60 | -0.08 | -4.8,-5.0 |
| | MgO | 4.27[67], 4.30[68], 4.43[69], 4.02[69] | -8.60 | -0.80 | -4.33, -4.30, -4.17, -4.58 |
| | α-$Ga_2O_3$ | 3.59[70] | -8.17 | -3.63 | -4.58 |
| | $GdAlO_3$ | 4.20[#] | -8.66 | -0.67 | -4.30 |
| | $BaTiO_3$ | 2.3[71] | -7.25 | -3.59 | -4.95 |
| $Cr^{3+}$ | α-$Al_2O_3$ | 6.94[22], 6.90[33] | -9.6 | -0.08 | -2.66, -2.70 |
| | β-$Ga_2O_3$ | 4.10[50] | -8.17 | -3.63 | -4.07 |
| | $ZnGa_2O_4$ | 4.56[51] | -8.40 | -3.50 | -3.84 |
| | $Y_3Al_5O_{12}$ | 6.66[##] | -9.38 | -1.71 | -2.72[#] |
| | MgO* | 6.80 | -8.82 | -0.28 | -2.02 |
| | $LaAlO_3$ | 5.28[72] | -7.82 | -1.22 | -2.54 |
| | $GdAlO_3$ | 6.36[73] | -8.66 | -0.92 | -2.30 |

*Here, the bandgap of MgO at room temperature is about 7.6 eV[74] and the $E_v$ can be deduced from the data in literature[75]. Its impurity level is about 0.8 eV below the conduction band of MgO[76]. So the VRBE of $Cr^{3+}$ in MgO would be at about -2.02 eV. Its CT value is about 6.8 eV, which is also listed in the table for completeness.

View Article Online
DOI: 10.1039/C8TC05401K

# See the experimental data in Electronic Supporting Information.

##This value is obtained from TL results [16].

Although the VRBEs of $Ti^{4+/3+}$, $Mn^{4+/3+}$, $Cr^{3+/2+}$ and $Fe^{3+/2+}$ in the listed compounds show a spread of about ±1 eV, their mean values still can offer a first estimate on the location of TM acceptor levels in compounds. For the average VRBEs of other 3d-TM ions, we could not obtain enough CT data to extract them. An alternative approach is to shift our OTL curves until the VRBEs of $Fe^{3+/2+}$ and $Mn^{4+/3+}$ evaluated from our calculation are consistent with the average values in Fig. 6(a, b), respectively. The results are shown in Fig.7 and Table 3. The VRBEs of $Ti^{4+/3+}$ and $Cr^{3+/2+}$ predicted from our VRBE curves is about -3.792 eV and -2.468 eV, and the corresponding experimental mean values are about -3.95 eV [49] and -2.49 eV. The VRBE of $Cr^{3+}$ impurity levels in $GdAlO_3$ and $LaAlO_3$ obtained through $Cr^{3+}$-CB electron transfer process are at about -6.2±0.2 eV and -6.3±0.2 eV respectively[73], which are also very close to our $Cr^{4+/3+}$ data of -6.235 eV. Such good agreement demonstrates that our VRBE curves in Fig. 7 also fit well with other 3d-TM ions in octahedral aluminates. Thus, the VRBE curves in Figure 6 can be used to roughly predict the acceptor levels of 3d-TM ions on octahedral sites in a giving aluminate.

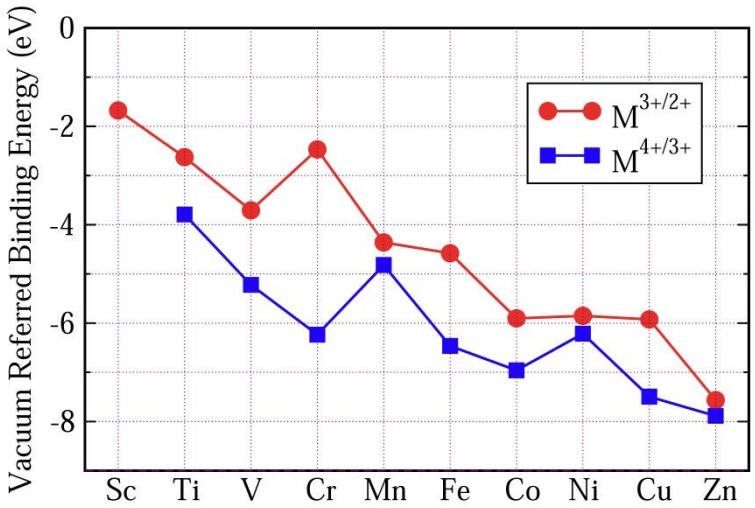


**Figure 7** (Color online) The average VRBE of 3d-TM ions in aluminates predicted from combining calculated OTL energies with experimental CT-energies.

**Table 3** The average VRBE of 3d-TM ions in aluminates predicted in this work. All energies are in eV.

| | $TM^{3+/2+}$ | $TM^{4+/3+}$ |
|---|---|---|
| **Sc** | -1.679 | --- |
| **Ti** | -2.626 | -3.792 |
| **V** | -3.709 | -5.221 |
| **Cr** | -2.468 | -6.235 |
| **Mn** | -4.360 | -4.820 |
| **Fe** | -4.580 | -6.464 |
| **Co** | -5.904 | -6.962 |
| **Ni** | -5.853 | -6.214 |
| **Cu** | -5.924 | -7.494 |
| **Zn** | -7.566 | -7.885 |

In an attempt to arrive at a more accurate prediction of VRBE, we studied the fluctuation of the 3d-TM VRBE in different aluminates. The dashed line in Fig. 8 shows that when the VRBE at the VBM increases, the VRBE of the $Mn^{4+/3+}$ acceptor level increases linearly with slope of about 0.74. The maximum deviation of the experimental VRBE of $Mn^{4+/3+}$ from the dashed line is 0.19 eV. So, the estimation of the VRBE of $Mn^{4+/3+}$ in an aluminate might be more accurately made if the VRBE of the VBM is known.

View Article Online
DOI: 10.1039/C8TC05401K

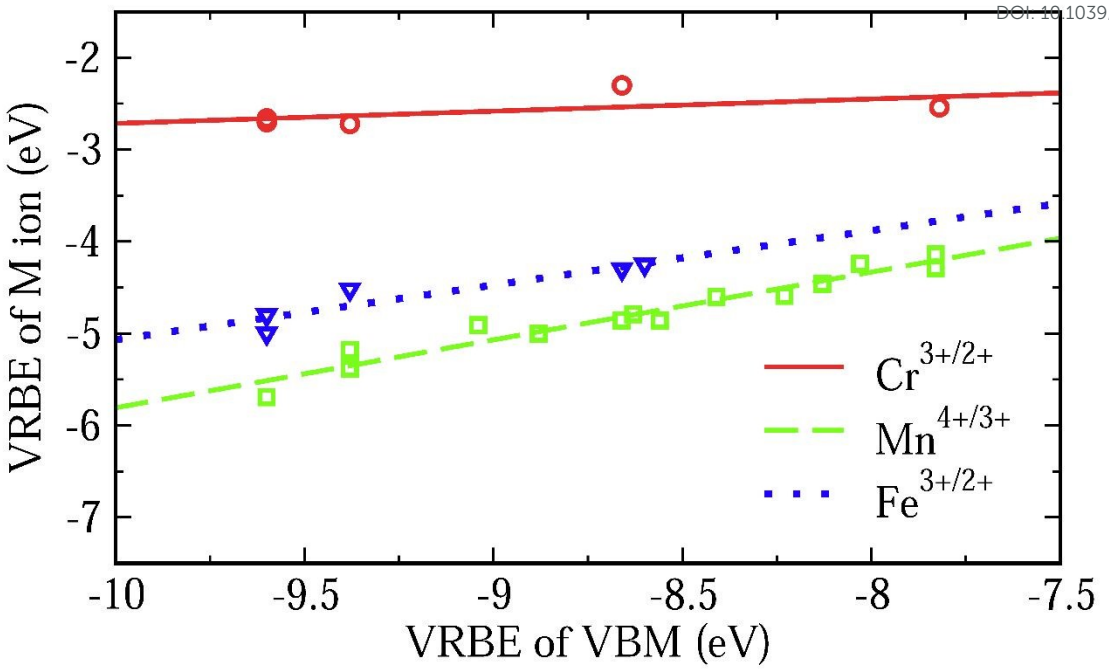


**Figure 8** (Color online) The VRBE of $Cr^{3+/2+}$, $Fe^{3+/2+}$ and $Mn^{4+/3+}$ as functions of VBM of different aluminates with octahedral site derived from Table 2.

The relationship between the VRBE of $Mn^{4+/3+}$ and VBM could be understood from the molecular orbital theory. As mentioned above, the VRBE of the Mn ion is dominated by the antibonding orbitals t* or e*. When raising the energies of ligand bonds, t* and e* orbitals increase in energy and so does the VRBE of Mn ion. Since the VB are mainly constructed by ligand bonds, the increase of the energies of ligand bonds can cause the VBM shifted upwards. So, the VRBE of $Mn^{4+/3+}$ increase with the increase of VBM. This rule can also be applied for the VRBEs of other 3d-TM ions. So, we fitted the VRBE of $Cr^{3+/2+}$ or $Fe^{3+/2+}$ to a straight line as shown by the solid or dotted line in Fig. 8. Their slopes are about 0.13 and 0.59 with the largest data deviations of about 0.23 eV and 0.18 eV, respectively. When more data are available these seemingly linear relationships can be tested further. Here we used the VBM as a variable but other aspects like the crystal field splitting of $3d^n$ level can also be important.

Finally, we will elaborate somewhat further on the charge states of M ions in compounds. When the energies of the 3d orbitals are higher than those of the ligand

bonds, t* and e* are mainly contributed by 3d orbtials. Sc, Ti, V, Cr, Mn, Fe and Co ions belong to this case, which can be proved by the PDOS in Fig. S2 to Fig. S8 of the ESI. So, the electrons in the t* and e* can be roughly regarded as the 3d electrons of M ions. The OTL and CT energies then reflect the location of the acceptor levels induced by the t* or e* orbitals and thus approximately reflect the VRBE of the 3d orbitals of M ions. So, we denote them as for example OTL($M^{3+/2+}$) or $E^{CT}$(M,3). When the atomic number increases from Sc to Zn, the energies in the 3d orbitals decrease and the contribution of ligand bonds (which are mostly O 2p orbitals) to the t* or e* orbitals increases. Especially, for the case of Zn, the defect levels are mostly contributed by O 2p orbitals, while the contribution of 3d orbitals concentrates on the bonding t and e orbitals, which are about 3 ~ 6.0 eV below the VBM. Now, the electrons in the t* and e* should be roughly regarded as the p electrons of O ions. Thus, the charge state of Zn ion is nearly unrelated to the defect levels in the band gap. In other words, the Zn ion should be approximately in the 2+ state in all the calculations (4s electrons have lost). However, the OTL and CT energies still reflect the locations of acceptor levels induced by t* or e* orbitals. Although the contribution of the 3d orbitals of Zn to the t* and e* orbitals is negligible small, the energies of 3d orbitals still can be can be considered part of the t* and e* orbitals. So, we adopted like OTL($Zn^{3+/2+}$) or $E^{CT}$(Zn,3) to denote the corresponding OTL and CT bands, nominally.

## Conclusion

In this work, we offer a method to predict the acceptor levels of 3d-TM ions in octahedral aluminates by constructing zig-zag like VRBE curves employing the experimental CT band energies of 3d-TM ions and by first-principle calculation. These curves offer a rough estimate about the acceptor level energies of 3d-TM ions with a spread of about ±1 eV. The estimation can be more accurate if we take molecular orbital theory into consideration without complicated calculations. Our work gives a vivid and quantitative explanation of how binding energy varies with the increase of n for 3d orbital electrons, and make it easier to estimate their doping levels in a specify

compound. Those predictable levels are very useful in engineering the luminescent properties of 3d-TM activated phosphors. For the phosphors with tetrahedral sites, such as silicates, (oxy)nitrides, we speculate similar rules may exist from the view of the molecular orbital theory, but the shape of the zig-zag-curve should be different from that in octahedral site as shown in Fig. 7. We need more experimental data to extract and verify them. This work is under way.

## Acknowledgments

This work is supported by the National Natural Science Foundation of China (Grant No: 51302059 and 11404085), NSAF (Grant No: U1630118), China Scholarship Council (201406695020) and the Natural Science Foundation of Anhui Province (Grant 1708085ME121). Calculations were done in the Supercomputing Center of University of Science and Technology of China.





1. S. Kück, *Appl. Phys. B*, 2001, **72**, 515-562.
2. Y. Hao and Y. Wang, *J. Lumin.*, 2007, **122-123**, 1006-1008.
3. W. Lü, W. Lv, Q. Zhao, M. Jiao, B. Shao and H. You, *Inorg. Chem.*, 2014, **53**, 11985-11990.
4. H.-D. Nguyen, C. C. Lin, M.-H. Fang and R.-S. Liu, *J. Mater. Chem. C*, 2014, **2**, 10268-10272.
5. L. Wang, Z. Dai, R. Zhou, B. Qu and X. C. Zeng, *Phys. Chem. Chem. Phys.*, 2018, **20**, 16992-16999.
6. Z. Pan, Y.-Y. Lu and F. Liu, *Nat. Mater.*, 2012, **11**, 58-63.
7. Y. Wang and L. Wang, *J. Appl. Phys.*, 2007, **101**, 053108-053105.
8. Z. Liu, L. Zhao, W. Chen, S. Xin, X. Fan, W. Bian, X. Yu, J. Qiu and X. Xu, *J. Am. Ceram. Soc.*, 2018, **101**, 3480-3488.
9. B. Qu, B. Zhang, L. Wang, R. Zhou and X. C. Zeng, *Chem. Mater.*, 2015, **27**, 2195-2202.
10. G. Blasse and B. Grabmaier, *Luminescent materials*, Springer, Berlin, 1994.
11. B. Qu, B. Zhang, L. Wang, R. Zhou, X. C. Zeng and L. Li, *ACS Appl. Mater. Interfaces*, 2016, **8**, 5439-5444.
12. P. Dorenbos, *Physical Review B*, 2012, **85**.
13. P. Dorenbos, *Physical Review B*, 2013, **87**, 035118.
14. E. G. Rogers and P. Dorenbos, *ECS J. Solid State Sci. Technol.*, 2014, **3**, R173-R184.
15. J. Ueda, A. Hashimoto, S. Takemura, K. Ogasawara, P. Dorenbos and S. Tanabe, *J. Lumin.*, 2017, **192**, 371-375.
16. J. Ueda, P. Dorenbos, A. J. J. Bos, K. Kuroishi and S. Tanabe, *J. Mater. Chem. C*, 2015, **3**, 5642-5651.
17. P. Dorenbos, *Opt. Mater.*, 2017, **69**, 8-22.
18. G. Kresse and J. Furthmüller, *Physical Review B*, 1996, **54**, 11169-11186.
19. G. Kresse and J. Hafner, *Physical review. B, Condensed matter*, 1993, **47**, 558-561.

View Article Online
DOI: 10.1039/C8TC05401K






20. J. P. Perdew, K. Burke and M. Ernzerhof, *Phys. Rev. Lett.*, 1996, **77**, 3865-3868.
21. C. G. V. d. Walle and J. Neugebauer, *J. Appl. Phys.*, 2004, **95**, 3851-3879.
22. H. H. Tippins, *Physical Review B*, 1970, **1**, 126-135.
23. D. S. McClure, *The Journal of Chemical Physics*, 1962, **36**, 2757-2779.
24. M. Kirm, G. Zimmerer, E. Feldbach, A. Lushchik, C. Lushchik and F. Savikhin, *Physical Review B*, 1999, **60**, 502-510.
25. V. Mürk and N. Yaroshevich, *physica status solidi (b)*, 1994, **181**, K37-K40.
26. Y. Zorenko, T. Zorenko, T. Voznyak, S. Nizhankovskiy, E. Krivonosov, A. Danko and V. Puzikov, *Opt. Mater.*, 2013, **35**, 2053-2055.
27. W. C. Wong, D. S. McClure, S. A. Basun and M. R. Kokta, *Physical Review B*, 1995, **51**, 5682-5692.
28. M. Yamaga, T. Yosida, S. Hara, N. Kodama and B. Henderson, *J. Appl. Phys.*, 1994, **75**, 1111-1117.
29. G. Molnár, M. Benabdesselam, J. Borossay, D. Lapraz, P. Iacconi, V. S. Kortov and A. I. Surdo, *Radiat. Meas.*, 2001, **33**, 663-667.
30. T. Huang, B. Jiang, Y. Wu, J. Li, Y. Shi, W. Liu, Y. Pan and J. Guo, *J. Alloys Compd.*, 2009, **478**, L16-L20.
31. J. P. Meyn, T. Danger, K. Petermann and G. Huber, *J. Lumin.*, 1993, **55**, 55-62.
32. M. J. Weber and L. A. Riseberg, *The Journal of Chemical Physics*, 1971, **55**, 2032-2038.
33. V. A. Pustovarov, V. S. Kortov, S. V. Zvonarev and A. I. Medvedev, *J. Lumin.*, 2012, **132**, 2868-2873.
34. S. Kück, K. Petermann, U. Pohlmann and G. Huber, *J. Lumin.*, 1996, **68**, 1-14.
35. Y. Xu, L. Wang, B. Qu, D. Li, J. Lu and R. Zhou, *J. Am. Ceram. Soc.*, 2018, **0**.
36. K. Petermann and G. Huber, *J. Lumin.*, 1984, **31–32, Part 1**, 71-77.
37. D. Q. Chen, Y. Zhou, W. Xu, J. S. Zhong, Z. G. Ji and W. D. Xiang, *J. Mater. Chem. C*, 2016, **4**, 1704-1712.
38. J. B. Blum, H. L. Tuller and R. L. Coble, *J. Am. Ceram. Soc.*, 1982, **65**, 379-382.
39. R. Moncorge, G. Boulon, D. Vivien, A. M. Lejus, R. Collongues, V. Djevahirdjian, K. Djevahirdjian and R. Gagnard, *IEEE J. Quantum Electron.*, 1988, **24**, 1049-1051.
40. C. Y. Chen, G. J. Pogatshnik, Y. Chen and M. R. Kokta, *Physical Review B*, 1988, **38**, 8555-8561.
41. K. Mori, *physica status solidi (a)*, 1977, **42**, 375-384.
42. I. S. Akhmadullin, S. A. Migachev and S. P. Mironov, *Nuclear Instruments and Methods in Physics Research Section B: Beam Interactions with Materials and Atoms*, 1992, **65**, 270-274.
43. S. R. Rotman, M. Roth, H. L. Tuller and C. Warde, *J. Appl. Phys.*, 1989, **66**, 1366-1369.
44. S. R. Rotman and H. L. Tuller, *J. Appl. Phys.*, 1987, **62**, 1305-1312.
45. N. Manuilov and P. Peshev, *Mater. Res. Bull.*, 1989, **24**, 1549-1555.
46. M. Yamaga, Y. Oda, H. Uno, K. Hasegawa, H. Ito and S. Mizuno, *J. Appl. Phys.*, 2012, **112**, 063508.
47. P. Hong, X. X. Zhang, C. W. Struck and B. D. Bartolo, *J. Appl. Phys.*, 1995, **78**, 4659-4667.
48. P. Dorenbos, *J. Lumin.*, 2013, **134**, 310-318.
49. E. G. Rogers and P. Dorenbos, *J. Lumin.*, 2014, **153**, 40-45.
50. H. Wakai, Y. Sinya and A. Yamanaka, *physica status solidi (c)*, 2011, **8**, 537-539.
51. A. Bessière, S. K. Sharma, N. Basavaraju, K. R. Priolkar, L. Binet, B. Viana, A. J. J. Bos, T. Maldiney, C. Richard, D. Scherman and D. Gourier, *Chem. Mater.*, 2014, **26**, 1365-1373.
52. E. G. Rogers and P. Dorenbos, *J. Lumin.*, 2014, **155**, 135-140.

53. Y. Li, Y.-Y. Li, K. Sharafudeen, G.-P. Dong, S.-F. Zhou, Z.-J. Ma, M.-Y. Peng and J.-R. Qiu, *Journal of Materials Chemistry C*, 2014, **2**, 2019-2027.
54. M. E. van Ipenburg, G. J. Dirksen and G. Blasse, *Mater. Chem. Phys.*, 1995, **39**, 236-238.
55. A. M. Srivastava and M. G. Brik, *Opt. Mater.*, 2017, **63**, 207-212.
56. L. Wang, Y. Xu, D. Wang, R. Zhou, N. Ding, M. Shi, Y. Chen, Y. Jiang and Y. Wang, *physica status solidi (a)*, 2013, **210**, 1433-1437.
57. T. Murata, T. Tanoue, M. Iwasaki, K. Morinaga and T. Hase, *J. Lumin.*, 2005, **114**, 207-212.
58. M. A. Noginov and G. B. Loutts, *Journal of the Optical Society of America B*, 1999, **16**, 3-11.
59. R. Cao, K. N. Sharafudeen and J. Qiu, *Spectrochimica Acta Part A Molecular & Biomolecular Spectroscopy*, 2014, **117**, 402-405.
60. M. Peng, X. Yin, P. A. Tanner, C. Liang, P. Li, Q. Zhang and J. Qiu, *J. Am. Ceram. Soc.*, 2013, **96**, 2870-2876.
61. M. Aoyama, Y. Amano, K. Inoue, S. Honda, S. Hashimoto and Y. Iwamoto, *Journal of Luminescence*, 2013, **136**, 411-414.
62. Y. Chen, M. Wang, J. Wang, M. Wu and C. Wang, *Journal of Solid State Lighting*, 2014, **1**, 15.
63. R. Cao, Q. Xiong, W. Luo, D. Wu, X. Fen and X. Yu, *Ceram. Int.*, 2015, **41**, 7191-7196.
64. G. Blasse and P. H. M. D. Korte, *Journal of Inorganic & Nuclear Chemistry*, 1981, **43**, 1505-1506.
65. T. R. N. Kutty and M. Nayak, *J. Alloys Compd.*, 1998, **269**, 75-87.
66. D. E. Lacklison, G. B. Scott and J. L. Page, *Solid State Commun.*, 1974, **14**, 861-863.
67. S. Clement and E. R. Hodgson, *Mrs Online Proceeding Library*, 2011, **60**.
68. A. M. Stoneham, M. J. L. Sangster and P. W. Tasker, *Philosophical Magazine Part B*, 1981, **44**, 603-613.
69. K. Dunphy and W. W. Duley, *J. Phys. Chem. Solids*, 1990, **51**, 1077-1082.
70. G. T. Pott and B. D. McNicol, *J. Lumin.*, 1973, **6**, 225-228.
71. A. Mazur, C. Veber, O. F. Schirmer, C. Kuper and H. Hesse, *Radiat. Eff. Defects Solids*, 1999, **150**, 281-286.
72. Y. Katayama, H. Kobayashi and S. Tanabe, *Appl. Phys. Express*, 2015, **8**, 012102.
73. H. Luo and P. Dorenbos, *J. Mater. Chem. C*, 2018, **6**, 4977-4984.
74. M. L. Bortz, R. H. French, D. J. Jones, R. V. Kasowski and F. S. Ohuchi, *Phys. Scr.*, 1990, **41**, 537.
75. P. Dorenbos, *J. Lumin.*, 2005, **111**, 89-104.
76. C. C. Chao, *J. Phys. Chem. Solids*, 1971, **32**, 2517-2528.

TOC

View Article Online
DOI: 10.1039/C8TC05401K

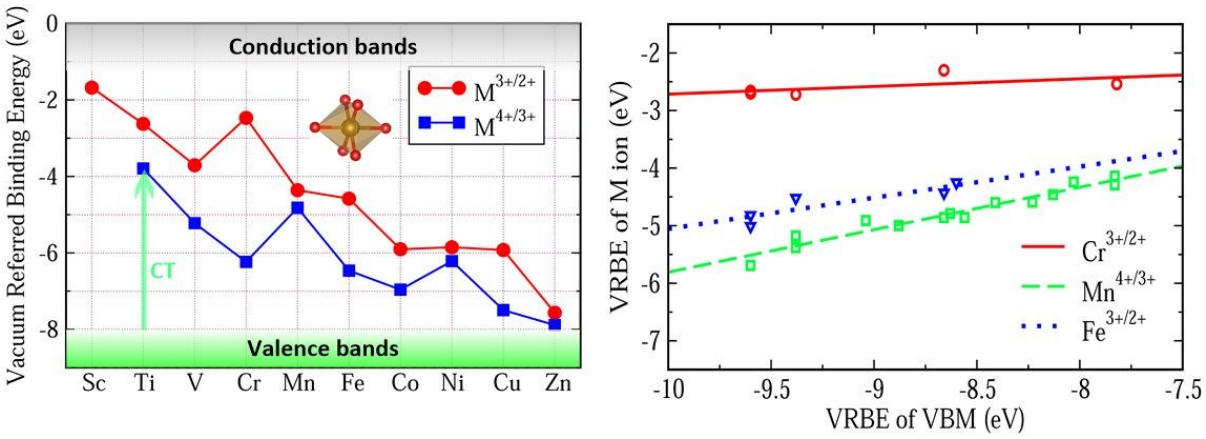


First estimate (left) and accurate estimate (right) of the defect levels of 3d-TM ions in octahedral sites of aluminate phosphors.